Separation Science and Technology
Publication details, including instructions for authors and subscription information:
http://www.informaworld.com/smpp/title~content=t713708471

THERMAL EFFECTS ON THE BREAKTHROUGH CURVE OF A HYDROGEN TERNARY SYSTEM AT A FIXED BED

Hyungwoong Ahn[a]; Choonsup Chun[a]; Myungkyu Park[a]; Ik-Sung Ahn[a]; Chang-Ha Lee[a]
[a] Department of Chemical Engineering, Yonsei University Shinchon-dong, Seoul, Korea

Online publication date: 31 August 2001

To cite this Article Ahn, Hyungwoong , Chun, Choonsup , Park, Myungkyu , Ahn, Ik-Sung and Lee, Chang-Ha(2001) 'THERMAL EFFECTS ON THE BREAKTHROUGH CURVE OF A HYDROGEN TERNARY SYSTEM AT A FIXED BED', Separation Science and Technology, 36: 10, 2121 — 2145
To link to this Article: DOI: 10.1081/SS-100105909
URL: http://dx.doi.org/10.1081/SS-100105909

SEPARATION SCIENCE AND TECHNOLOGY, 36(10), 2121–2145 (2001)

THERMAL EFFECTS ON THE BREAKTHROUGH CURVE OF A HYDROGEN TERNARY SYSTEM AT A FIXED BED

Hyungwoong Ahn, Choonsup Chun, Myungkyu Park, Ik-Sung Ahn and Chang-Ha Lee*

Department of Chemical Engineering,
Yonsei University Shinchon-dong, Seodaemun-gu,
Seoul, 120-749, Korea

ABSTRACT

The thermal effect on the breakthrough curve of a hydrogen ternary mixture ($H_2/CH_4/CO$; 60:30:10 vol%) was investigated experimentally and theoretically at a fixed bed in the range of 4 to 16 kg_f/cm^2 adsorption pressure and 4.5–9.1 LSTP/min feed flow rate. To understand the adsorption dynamics and the thermal effect by the heat of adsorption, a non-isothermal dynamic model incorporating mass, energy, and momentum balances was used and was compared with isothermal and adiabatic models. The adsorption thermal effects on adsorption dynamics were compared between an activated carbon bed and a zeolite 5A bed. In the activated carbon bed, the roll-up of CO by CH_4 and the separation of mass transfer zones between CO and CH_4 occurred and the H_2 breakthrough curve showed a stepwise decrease and tailing. However, a

*Corresponding author. Fax: +82-2-312-6401; E-mail: leech@yonsei.ac.kr

small roll-up of CH_4 and a wide breakthrough of CO in the experimental range was shown in the zeolite bed without the separation of two temperature wave fronts. The breakthrough time was elongated by an increase in adsorption pressure and by a decrease in feed flow rate in each adsorbent bed, but the extent of elongation was different due to the difference between the affinities of CO and CH_4 to each adsorbent. Also, in the activated carbon bed, the extent of roll-up became wider with a decrease in feed flow rate and became steeper with an increase in adsorption pressure. Depending on the thermal condition in each bed, concentration and temperature profiles showed different behavior.

Key Words: Adsorption dynamics; Hydrogen ternary mixture; Roll-up phenomenon; Breakthrough curve; Temperature excursion

INTRODUCTION

Fixed-bed adsorption process has been an important unit operation for purification and bulk separation of gas mixture. In recent years, it has increasingly been applied to a large-scale separation process. One of the successful applications of a pressure swing adsorption (PSA) process is hydrogen recovery because a high-purity H_2 product with high productivity can be obtained from a well-designed PSA.

Recently, various PSA processes with layered beds or with two groups of a single-adsorbent bed have been studied extensively (1–6). The key step to developing an optimum PSA process lies in the design and operation of the adsorption step. Therefore, given quite a few experimental results of adsorption breakthrough by which the adsorption step in the PSA process could be predictable, such useful information as breakthrough time, adsorption dynamics and the amount of heat release can be used to develop a novel PSA process. Also, on the condition that the theoretical models of the adsorption breakthrough can predict its experimental results well, it can be used to investigate the breakthrough dynamics in a bed and predict PSA performance without any specific experiment.

After the study by Sircar and Kumar (7,8) on the constant pattern adiabatic adsorption from bulk single-component and binary gas mixtures, the adsorption dynamics for a fixed-bed bulk component system has been studied extensively (9–12). In a multi-component mixture, the breakthrough behavior generally includes a roll-up or plateau phenomenon and temperature variation in the bed. Since a roll-up phenomenon reflects competitive adsorption caused by different equilibrium affinity of each component for an adsorbent, the complexity peculiar to a specific adsorbate–adsorbent system can be expected (12). Some researchers pointed

MARCEL DEKKER, INC.
270 Madison Avenue, New York, New York 10016

out that roll-up can take place in an equilibrium control system as well as in a kinetically controlled system (13). Recently, Park and coworkers (11) reported that multiple roll-ups in the equilibrium separation system could be stemmed not only from different equilibrium affinity but also from sorption kinetics.

In this study, the adsorption dynamics of ternary hydrogen mixture ($H_2/CH_4/CO$; 60.4:28.1:11.5 vol%) in activated carbon and zeolite 5A beds were investigated through breakthrough experiments. The experimental results and dynamics in the bed were analyzed by using a non-isothermal dynamic model incorporating mass, energy, and momentum balances. Although the temperature increase inside a bed is undesirable, temperature variation during the adsorption process is inevitable. Therefore, the adsorption dynamics and roll-up phenomenon in each bed were investigated according to the relationship between the concentration and temperature profiles. These experimental results were also compared with the simulated results in the isothermal and adiabatic conditions.

EXPERIMENTAL STUDIES

The ternary hydrogen mixture ($H_2/CH_4/CO$; 60.4:28.1:11.5 vol%) was used as feed gas. Activated carbon (6–16 mesh, Calgon Co.) and zeolite 5A (4–8 mesh, W. R. Grace Co.) were used in a breakthrough experiment. Before the experiment, the activated carbon and the zeolite 5A were regenerated for more than 12 h at 323 and 593 K, respectively. The characteristics of adsorbents are shown in Table 1.

The schematic diagram of an experimental apparatus is shown in Fig. 1. The adsorption bed was made of stainless steel of 100 cm length and 3.71 cm ID. To measure the temperature inside the bed, four RTDs were installed at the position of 10, 30, 50, and 75 cm from the feed end. The pre-calibrated mass flow controller (F-201C, Bronkhorst High-Tech) was installed between a feed tank and an adsorption bed to control the feed flow rate. The total amount of gas was confirmed by a wet gas meter (W-NK-1B, Shinagawa). The electrical back-pressure regulator between the adsorption bed and the product tank was installed to main-

Table 1. Characteristics of Adsorbents

Type	Activated Carbon	Zeolite5A
	Granular	Sphere
Pellet size [mesh]	6–16	4–8
Pellet density [g/cm^3]	0.85	1.16
Bulk density [g/cm^3]	0.482	0.746
Bed porosity [−]	0.433	0.357
Total void fraction [−]	0.78	0.77
Heat capacity [cal/g·K]	0.25	0.22

MARCEL DEKKER, INC.
270 Madison Avenue, New York, New York 10016

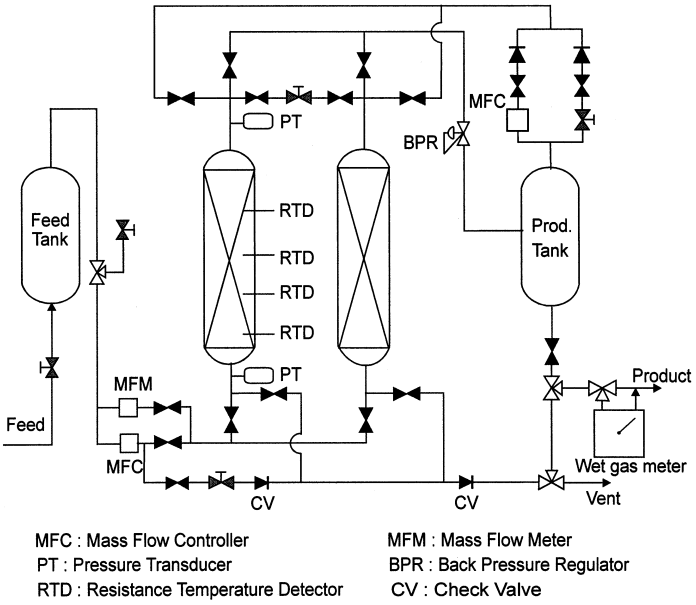

Figure 1. Schematic diagram of apparatus for breakthrough experiments.

tain constant adsorption pressure in the bed. Effluent stream was sampled between the back-pressure regulator and the product tank and was analyzed by using a mass spectrometer (QME 200, Balzers). All the data including concentration, temperature, pressure, and flow rate were saved on the computer.

The breakthrough experiments were performed in the range of 4.5, 6.8, and 9.1 LSTP/min feed flow rate and 4, 10, and 16 kg_f/cm^2 adsorption pressure. The adsorption bed was initially saturated with H_2 at the adsorption pressure.

MATHEMATICAL MODEL

To understand the adsorption dynamics, a non-isothermal dynamic model was applied with the following assumptions : 1) The flow pattern can be described by an axially dispersed plug flow model. 2) The ideal gas law can be applied. 3) The solid and gas phases reach a thermal equilibrium instantaneously. 4) Axial conduction in the column wall can be neglected. 5) Radial concentration and temperature gradients in the adsorption bed are negligible. 6) Second order concentration gradient is negligible in the overall mass balance. These assumptions have been widely accepted by numerous studies in the adsorption process (5,11,13,14).

MARCEL DEKKER, INC.
270 Madison Avenue, New York, New York 10016

The component mass balance with axial dispersion term was used to calculate concentration in the gas bulk phase.

$$-D_L\frac{\partial^2 c_i}{\partial z^2}+\frac{\partial(uc_i)}{\partial z}+\frac{\partial c_i}{\partial t}+\rho_p\left(\frac{1-\varepsilon}{\varepsilon}\right)\frac{\partial \bar{q}_i}{\partial t}=0 \tag{1}$$

where D_L is axial dispersion coefficient calculated by following a Wakao Eq. (15).

$$\frac{D_L}{2uR_P}=\frac{20}{\mathrm{Re}\,Sc}+0.5$$

The overall mass balance was used to calculate interstitial velocity (u) by the following equation.

$$\frac{\partial C}{\partial t}+\frac{\partial(uC)}{\partial z}+\frac{1-\varepsilon}{\varepsilon}\rho_p\sum_{i=1}^{n}\frac{\partial \bar{q}_i}{\partial t}=0 \tag{2}$$

Assuming instant thermal equilibrium between fluid and particles, the energy balance in the gas and solid phases was given by

$$-K_L\frac{\partial^2 T}{\partial z^2}+(\varepsilon_t\rho_g C_{pg}+\rho_B C_{ps})\frac{\partial T}{\partial t}+\rho_g C_{pg}\varepsilon u\frac{\partial T}{\partial z}-\rho_B\sum_{i=1}^{n}Q_i\frac{\partial \bar{q}_i}{\partial t}+\frac{2h_i}{R_{Bi}}(T-T_w)=0 \tag{3}$$

where K_L is the effective axial thermal conductivity (16).

In this study, the heat loss through a column wall cannot be neglected because the ratio of column length to diameter is large. Therefore, the energy balance in the column wall was used as follows.

$$\rho_w C_{pw}A_w\frac{\partial T_w}{\partial t}=2\pi R_{Bi}h_i(T-T_w)-2\pi R_{Bo}h_o(T_w-T_{atm}) \tag{4a}$$

$$A_w=\pi(R_{Bo}^2-R_{Bi}^2) \tag{4b}$$

To calculate the pressure drop along the bed, Ergun's equation was used (17).

$$-\frac{dP}{dz}=a\mu\nu+b\rho\nu|\nu| \tag{5a}$$

$$a=\frac{150}{4R_P^2}\frac{(1-\varepsilon)^2}{\varepsilon^3},\qquad b=1.75\frac{(1-\varepsilon)}{2R_P}\varepsilon^3 \tag{5b}$$

where ν is superficial velocity.

In this study, the following loading ratio correlation (LRC) and a linear driving force (LDF) model were used for the adsorption equilibrium and sorption rate, respectively (5,12).

$$q_i^* = \frac{q_{mi} B_i P_i^{n_i}}{1 + \sum_{j=1}^{n} B_j P_j^{n_j}} \tag{6a}$$

$$q_m = k_1 + k_2 T, \quad B = k_3 e^{k_4/T}, \quad n = k_5 + k_6/T \tag{6b}$$

$$\frac{\partial \bar{q}_i}{\partial t} = \omega_i (q_i^* - \bar{q}_i) \tag{7}$$

And the well-known Danckwerts' boundary conditions were applied to solve the equations.

$$-D_L \left(\frac{\partial c_i}{\partial z}\right)\Big|_{z=0} = u(c_i|_{z=0^-} - c_i|_{z=0^+}); \qquad \left(\frac{\partial c_i}{\partial z}\right)\Big|_{z=L} = 0 \tag{8a}$$

$$-K_L \left(\frac{\partial T}{\partial z}\right)\Big|_{z=0} = \rho_g (c_p)_g u(T)|_{z=0^-} - T|_{z=0^+}); \qquad \left(\frac{\partial T}{\partial z}\right)\Big|_{z=L} = 0 \tag{8b}$$

where $c_i\big|_{z=0}$ means feed concentration for component i.

In the present study, a three-point backward finite difference method was applied for temporal derivative. And a second-order central difference and a second-order backward difference were used to approximate second-order and first-order spatial derivatives, respectively (17). The resultant finite difference equation came to have tridiagonal matrix in the left hand, and it can be solved rapidly by a tridiagonal matrix method. The same input parameters were used in the previous work (12,18).

RESULTS AND DISCUSSION

Effect of Non-isothermality on Breakthrough Curves in an Activated Carbon Bed

Figures 2 to 5 show the results of the breakthrough experiment and simulation of hydrogen mixture in the activated carbon bed under 10 kg_f/cm^2 adsorption pressure, 6.8 LSTP/min feed flow rate and 289.1 K. As shown in these figures, the experimental results agreed well with the simulated results.

In Fig. 2, the roll-up of CO breakthrough curve was due to a great difference in the equilibrium affinity of CO and CH_4 for the activated carbon (12). In the CO plateau, the CO concentration increased slightly with time. Then, it began to decrease with a small tail at the beginning of the breakthrough of CH_4. In case of H_2, the breakthrough curve dropped dramatically at the early breakthrough of CO and then decreased smoothly at the plateau of CO roll-up until the breakthrough of CH_4 occurred. The H_2 breakthrough curve showed tailing as the concentrations of

MARCEL DEKKER, INC.
270 Madison Avenue, New York, New York 10016

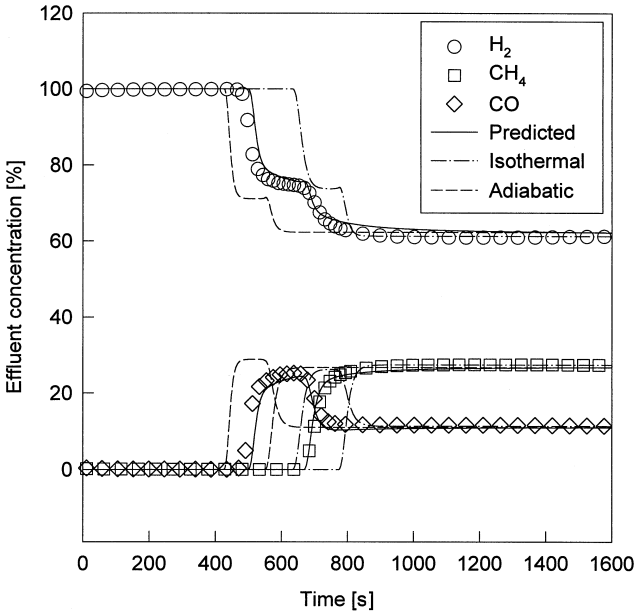

Figure 2. Experimental and simulated concentration breakthrough curves under 10 kg_f/cm^2 adsorption pressure and 6.8 LSTP/min feed flow rate (adsorption bed was initially saturated with H_2 at 10 kg_f/cm^2 and 289.1 K) in the activated carbon bed.

CO and CH_4 approached the feed compositions. Also, Fig. 2 shows the corresponding simulated breakthrough curves under the isothermal and adiabatic conditions. While the isothermal breakthrough curve was elongated around 140 s from the non-adiabatic and non-isothermal one, the breakthrough of CO in the adiabatic condition took place around 70 s earlier than the non-adiabatic and non-isothermal one. It implied that the experimental breakthrough time in this study was more similar to the adiabatic condition than the isothermal condition due to the difficulty in the heat transfer of the generated heat of adsorption. However, the extent of roll-up in the non-adiabatic and non-isothermal condition was more similar to the isothermal result than to the adiabatic result, whereas the shape of the plateau was different from the isothermal and adiabatic results.

In the isothermal condition, the adsorption amount of CO and CH_4 was relatively large due to a constant low bed-temperature. In the roll-up of CO, the adsorbed amount of CO in the isothermal condition was larger than those in other conditions because of the increased CO concentration and low bed-temperature. It is expected that this phenomenon in the isothermal condition will lead to a similar extent of CO roll-up in the non-isothermal and non-adiabatic condition. On the

MARCEL DEKKER, INC.
270 Madison Avenue, New York, New York 10016

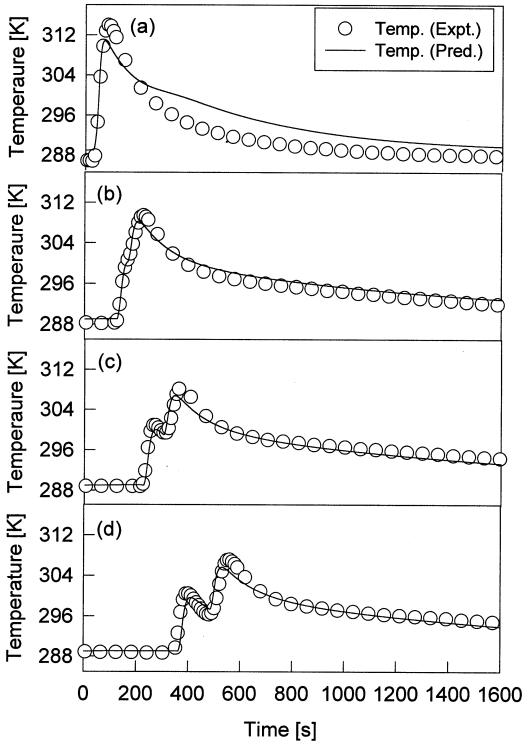

Figure 3. Temperature history at the position of (a) 10, (b) 30, (c) 50, and (d) 75 cm from the feed end under 10 kg_f/cm^2 adsorption pressure and 6.8 LSTP/min feed flow rate in the activated carbon bed.

contrary, the extent of roll-up of CO in the adiabatic condition was larger than that in the isothermal condition due to a decrease in adsorption capacity with temperature rise.

Meanwhile, in the non-isothermal and non-adiabatic condition, the desorption amount of CO by CH_4 adsorption was similar to that in the adiabatic condition due to a temperature increase. However, the adsorption of CO in the range of its roll-up was greater than that in the adiabatic condition because of the temperature decrease with the heat transfer to the outside of the bed. Therefore, the roll-up behavior of CO was broader than those in both adiabatic and isothermal conditions, and the plateau in the CO roll-up showed an increasing slope that was different from other conditions. Their detailed results will be explained with concentration and temperature profiles inside the bed later.

As the concentration wave fronts of CO and CH_4 propagated along the bed, the heat of adsorption brought the temperature rise in the bed. Temperature histo-

ries at 10, 30, 50, and 75cm from the feed end are presented in Fig. 3. In Fig. 3(a), temperature at the feed end decreased rapidly after the steep temperature excursion. The experimental temperature decreased more rapidly than the predicted one because of the heat loss at the flange of the adsorption bed and a small pressure shock at the feed end. This discrepancy has already been pointed out by a few researchers who asserted that the heat loss through the column inlet and outlet sections could have a strong effect on temperature predictions (11,19). However, experimental results agreed well with the predicted results in other locations. In Fig. 3(b), temperature history shows small inflection at around 150 s, which is different than Fig. 3(a). Since the CO and CH_4 wave fronts were close to each other

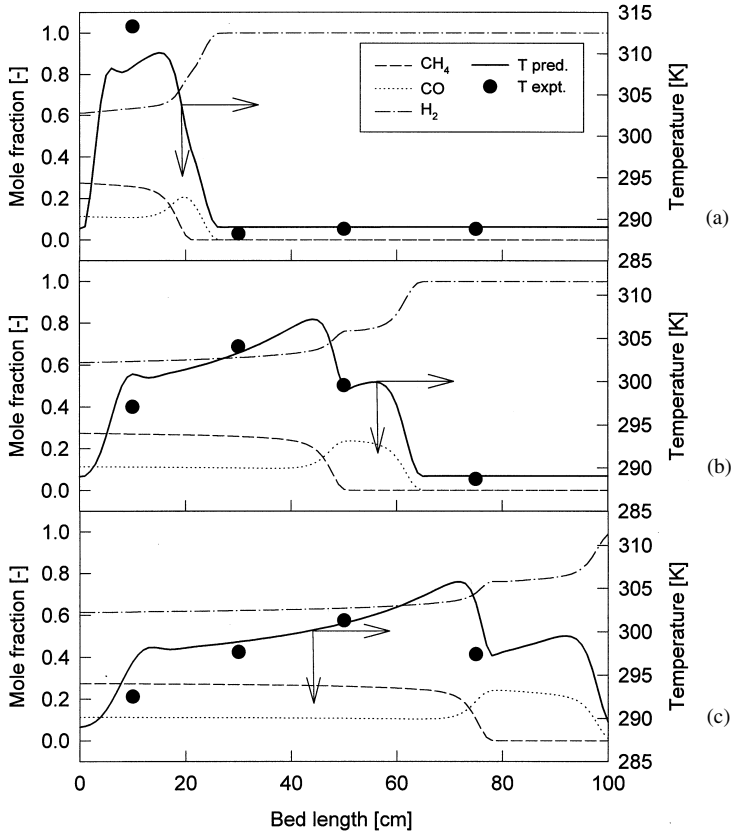

Figure 4. Concentration and temperature profiles in the gas phase at (a) 100, (b) 300, and (c) 500 s under 10 kg_f/cm^2 adsorption pressure and 6.8 LSTP/min feed flow rate in the activated carbon bed.

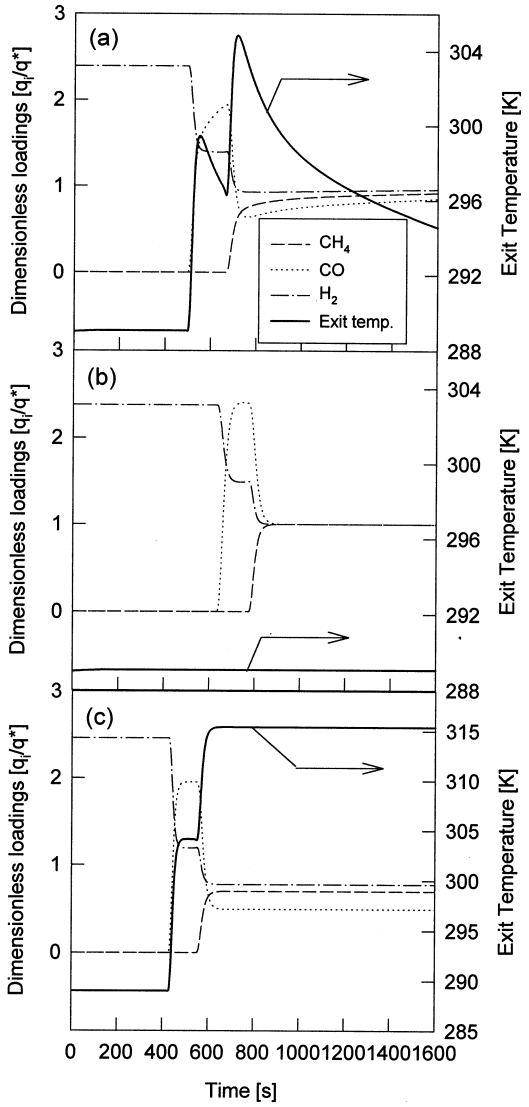

Figure 5. Dimensionless loadings in the solid phase and temperature history at the product end under 10 kg_f/cm^2 adsorption pressure and 6.8 LSTP/min feed flow rate in the activated carbon bed under (a) nonisothermal and nonadiabatic, (b) isothermal, and (c) adiabatic conditions.

at that location, the heat generation by the adsorption of CO and CH_4 took place almost simultaneously. However, the two temperature excursion peaks can be clearly seen in Fig. 3, (c) and (d). The first temperature peak was caused by the adsorption of CO and the latter by the adsorption of CH_4. The concentration wave fronts of CO and CH_4 got more and more separated due to different wave velocities of CO and CH_4 as they propagated along the bed. Therefore, the separated thermal wave fronts by the separated concentration wave fronts and heat transfer to the outside of the adsorption bed led to two temperature excursions in the temperature profile.

To show a clearer insight of this phenomenon, concentration and temperature profiles and dimensionless loadings are presented in Figs. 4 and 5, respectively. In Fig. 4(a), as the concentration wave fronts of CO and CH_4 propagated along the bed, heat loss of H_2 desorption and heat generations of CO and CH_4 adsorption occurred simultaneously at the beginning of the breakthrough. However, the net heat change caused the temperature to increase because of large heat generations of adsorption of CO and CH_4. At that location, the concentration wave fronts of CO and CH_4 at 100 s were close as mentioned in Fig. 3. However, as clearly seen in Fig. 4, (b) and (c), the two concentration wave fronts of CO and CH_4 in the gas phase were separated along the bed. Also, the difference between the propagation velocities of CO and that of CH_4 became greater with time. The well-known roll-up phenomenon in Fig. 4 results from the fact that weakly adsorbed components lose their adsorption sites due to the competitive adsorption of more strongly adsorbed components that follow the preceding wave fronts of weakly adsorbed components (2). Therefore, the desorbed CO joins the bulk stream and the CO concentration in the bulk stream becomes greater than that in the feed concentration. After the sharp CO wave front passed away, the bed temperature decreased due to the heat transfer to the outside of the bed. However, it increased again as the following CH_4 wave front propagated along the bed. As a result, the overall temperature profile and H_2 concentration wave front showed a stepwise form over the bed and the ravine between two temperature peaks became deeper with time as shown in Fig. 3.

Figure 5(a) shows the relationship between dimensionless loadings in the solid phase and time as well as that between temperature and time at the product end under the non-adiabatic and non-isothermal condition. After the H_2 loading showed a steep decrease in front of the mass transfer zone (MTZ) of CO, the inflection of H_2 loading occurred at the plateau of CO roll-up. Also, before the breakthrough of CH_4, the roll-up of CO occurred. Because of heat transfer to the outside of the bed and the increased CO concentration in the CO roll-up, it made a favorable condition for CO adsorption. Therefore, Fig. 4(c) shows that the adsorption of CO occurred in the plateau of roll-up but its loading amount decreased smoothly along the bed due to the temperature rise by its heat of adsorption. Then, it led a slope of the plateau in the CO roll-up in this system in Fig. 2, and the CO

MARCEL DEKKER, INC.
270 Madison Avenue, New York, New York 10016

loading showed an increasing trend with time at the CO plateau in Fig. 5(a). As the CH_4 wave front approached the product end, the H_2 loading decreased steeply again, and the bed temperature increased up to around 305 K. As a result, CO was desorbed steeply and the loading amount of CO became minimum near the second temperature peak. Then, the loadings of CO and CH_4 gradually approached the equilibrium loadings at the feed temperature as the temperature in the bed decreased again by heat transfer. This smooth increase in loading caused the tailing of H_2 breakthrough curve in Fig. 2.

However, under the isothermal condition in Fig. 5(b), the shape of CO roll-up was different from that in Fig. 5(a). Since there is no adsorption thermal effect, the CO loading at its plateau remained constant and the CO and CH_4 loadings remained constant after finishing the breakthrough of CH_4. Also, because there could not be any heat transfer through the wall in the adiabatic condition, the stepwise temperature profile by both breakthrough curves can be seen in Fig. 5(c). Therefore, the CO loading and temperature excursion kept constant at the CO plateau until the breakthrough of CH_4 occurred. Also, even after the breakthrough of CH_4, the loadings of all components were smaller than those in Fig. 5, (a) and (b), until the bed temperature returned to the feed temperature. In case of the adiabatic condition, the bed temperature was cooled by a feed gas flow because of no heat transfer outside the bed. Hence, the decreasing rate of temperature depended on the heat capacity of the mixture gas (C_{pg}) and the density of mixture gas (ρ_g). In this case, the exit temperature began to decrease near 5000 s and returned to the feed temperature at 7000 s due to the heat transfer by feed gas flow.

Effect of Non-Isothermality on Breakthrough Curves in a Zeolite 5A Bed

The adsorption equilibrium capacity of CH_4 on zeolite 5A was slightly larger than that of CO but the difference between the adsorption equilibrium capacities of CH_4 and CO on zeolite 5A is much smaller than that on the activated carbon (12). Therefore, contrary to the behavior in the activated carbon bed, CH_4 with higher partial pressure was the first breakthrough component followed by CO at short intervals in the zeolite 5A bed as shown in Fig. 6. Since both wave fronts of CH_4 and CO in the zeolite bed proceeded almost simultaneously, there was a small roll-up of CH_4 and wide breakthrough of CO. Also, the small inflection of H_2 breakthrough curve stemmed from the roll-up of CH_4.

Due to the variation of adsorption capacity by temperature, it took 75 s longer for the breakthrough of CH_4 to occur under the isothermal condition than under the non-isothermal and non-adiabatic condition. The breakthrough of CH_4 under the adiabatic condition occurred 35 s earlier than that under the non-isothermal and non-adiabatic condition. The changes in the adsorption capacity of CO and CH_4 with

MARCEL DEKKER, INC.
270 Madison Avenue, New York, New York 10016

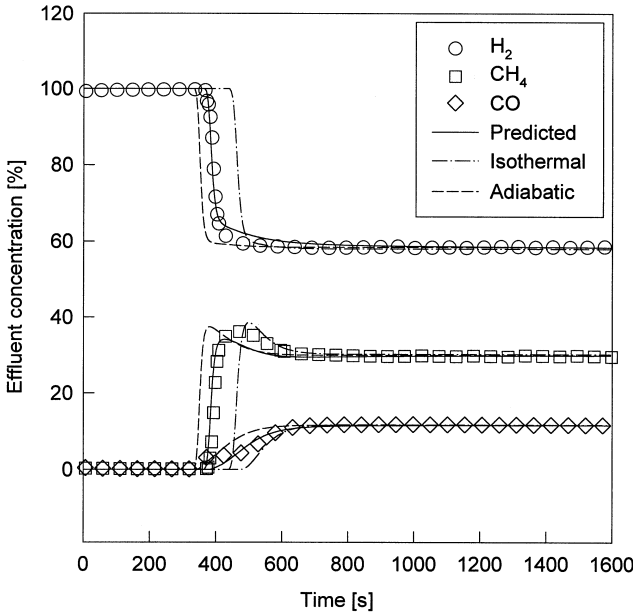

Figure 6. Experimental and simulated concentration breakthrough curves under 10 kg_f/cm^2 adsorption pressure and 6.8 LSTP/min feed flow rate (adsorption bed was initially saturated with H_2 at 10 kg_f/cm^2 and 289.1 K) in the zeolite 5A bed.

temperature in the zeolite bed were very small compared with that in the activated carbon bed. Therefore, the breakthrough time difference in the zeolite bed under the three different conditions was less than that in the activated carbon bed. Also, in Fig. 6, the breakthrough curve in the non-isothermal and non-adiabatic condition showed a smaller roll-up of CH_4 than that in the adiabatic condition because the heat transfer through the wall made a favorable condition for the adsorption of CH_4. However, the roll-up of CH_4 in the isothermal condition was similar to that in the adiabatic condition because of the high temperature dependency of the adsorption affinity in the zeolite 5A bed, which is different than Fig. 2 in the activated carbon bed.

Similar adsorption dynamics can be seen at the temperature history of a zeolite 5A bed in Fig. 7. There was hardly an inflection or two temperature excursion peaks in a zeolite 5A bed unlike that in the activated carbon bed. The maximum temperature at each position was higher than that in the activated carbon. This was because MTZs of CH_4 and CO propagated along the bed simultaneously with similar velocity.

Concentration and temperature profiles and dimensionless loadings in a zeolite 5A bed are presented in Figs. 8 and 9, respectively. In Fig. 8, the concentration wave fronts of CH_4 and CO proceeded almost simultaneously, contrary to

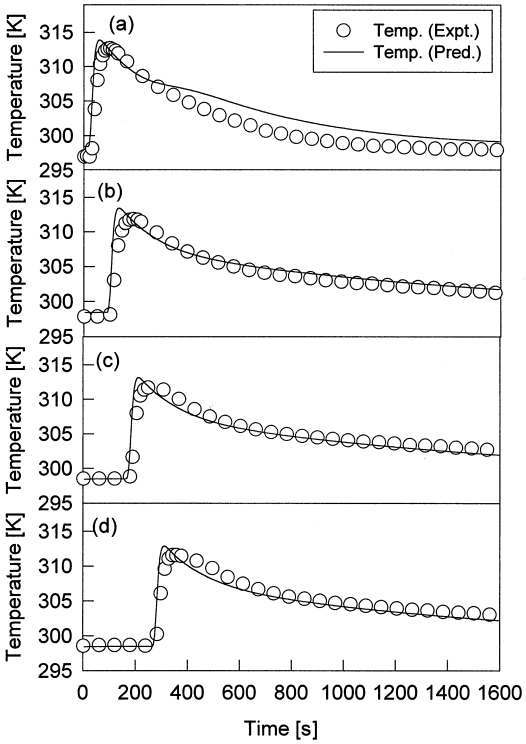

Figure 7. Temperature history at the position of (a) 10, (b) 30, (c) 50, and (d) 75 cm from the feed end under 10 kg_f/cm^2 adsorption pressure and 6.8 LSTP/min feed flow rate in the zeolite 5A bed.

those of the activated carbon bed. In addition, the small roll-up of CH_4 was observed by the wide CO concentration wave front. Therefore, the plateau of temperature profile showed a smooth increase without any inflection or variation, and H_2 concentration wave front propagated without any stepwise change. Also, the concentration wave fronts of CH_4 and CO propagated faster in the zeolite 5A bed than in the activated carbon bed.

In Fig. 9(a), before finishing the temperature increase by the adsorption of CH_4, the loading of CO began and a small roll-up of CH_4 occurred. Moreover, there was no double peak in temperature history. Then, the loading of CH_4 in the solid phase near the temperature peak (400 s) was slightly decreased by the heat of adsorption and CO loading. The loading of CO began to increase smoothly at the maximum loading of CH_4 and the peak of temperature excursion. After the crossover of the loading of CH_4 to CO, the loading of CO was slightly increased again by a decrease in temperature. As a result, the tailing of H_2 in the zeolite 5A bed was shorter than that in the activated carbon bed.

However, under the isothermal condition in Fig. 9(b), the roll-up of CH_4 and breakthrough of CO in the solid phase were steeper than those in Fig. 9(a) because there was no thermal effect by adsorption. Also, the CH_4 loading in the range of the CH_4 roll-up was greater in the isothermal condition than that in non-isothermal and non-adiabatic condition due to a low temperature in the bed. Under the adiabatic condition in Fig. 9(c), the CH_4 loading at the CH_4 roll-up was as small as that in the non-isothermal and non-adiabatic conditions because of a drastic temperature rise. As a result, the roll-up of CO in the adiabatic condition was similar to that in the isothermal condition in Fig. 6. After the breakthrough of CO, the bed temperature decreased very slowly due to the same reason as that for the activated carbon bed in Fig. 5. However, CO in the zeolite bed approached unity faster than CH_4 unlike the behavior on the activated carbon bed in Fig. 5, because

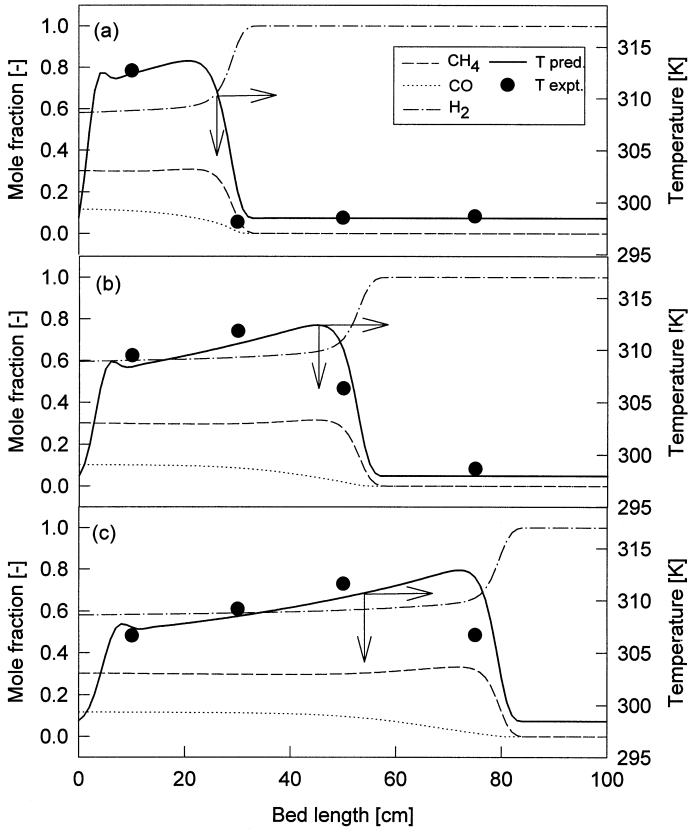

Figure 8. Concentration and temperature profiles in the gas phase at (a) 100, (b) 300, and (c) 500 s under 10 kg_f/cm^2 adsorption pressure and 6.8 LSTP/min feed flow rate in the zeolite 5A bed.

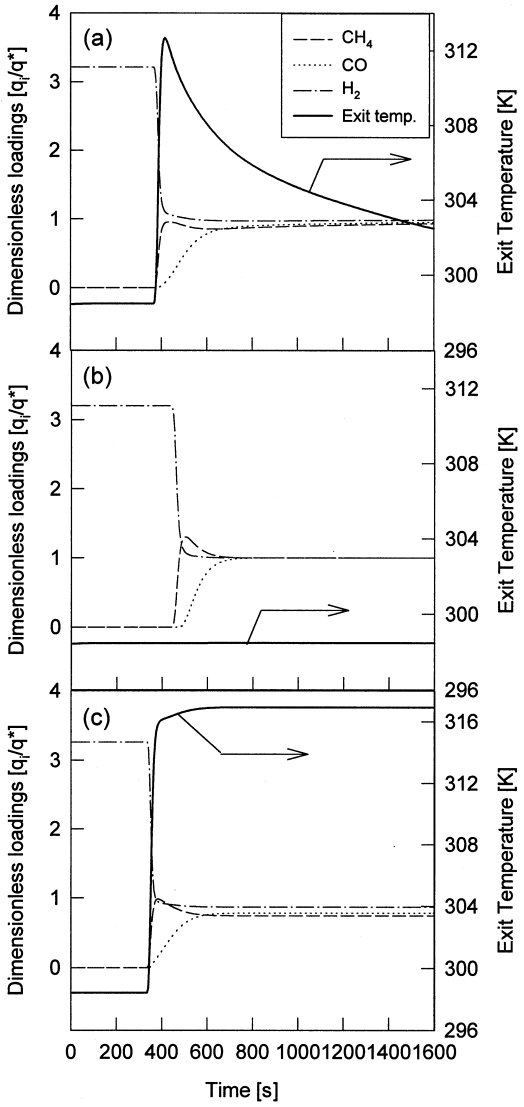

Figure 9. Dimensionless loadings in the solid phase and temperature history at the product end under 10 kg_f/cm^2 adsorption pressure and 6.8 LSTP/min feed flow rate in the zeolite 5A bed under (a) nonisothermal and nonadiabatic, (b) isothermal, and (c) adiabatic conditions.

the dependency of adsorption capacity of each component upon temperature was different according to the adsorbent.

Effect of Adsorption Pressure and Feed Rate on the Activated Carbon and Zeolite 5A Beds

The effects of feed flow rate and adsorption pressure on breakthrough curves in the activated carbon bed are presented in Figs. 10 and 11, respectively.

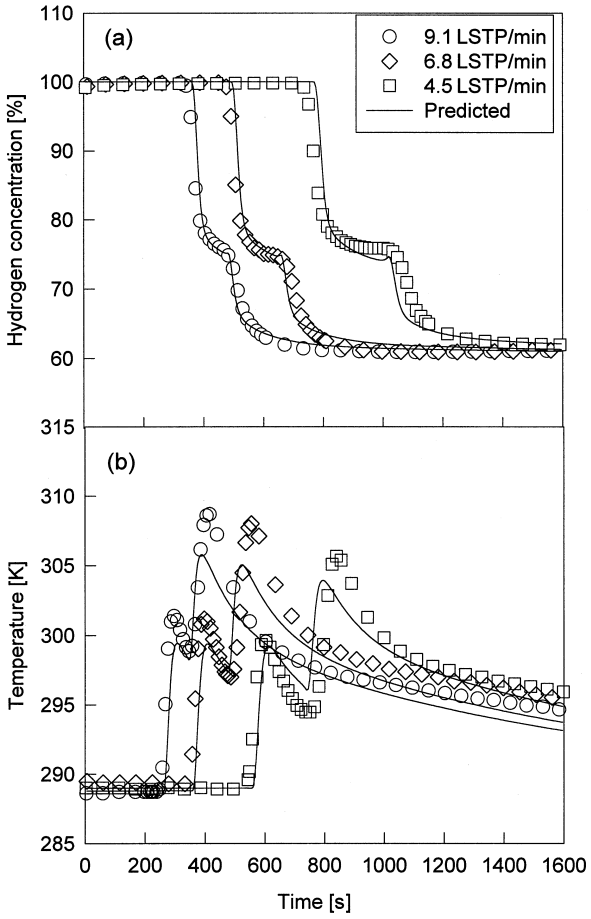

Figure 10. (a) Effect of feed flow rate on H_2 breakthrough curves at constant 10 kg_f/cm^2 adsorption pressure and (b) corresponding temperature profiles in the activated carbon bed.

MARCEL DEKKER, INC.
270 Madison Avenue, New York, New York 10016

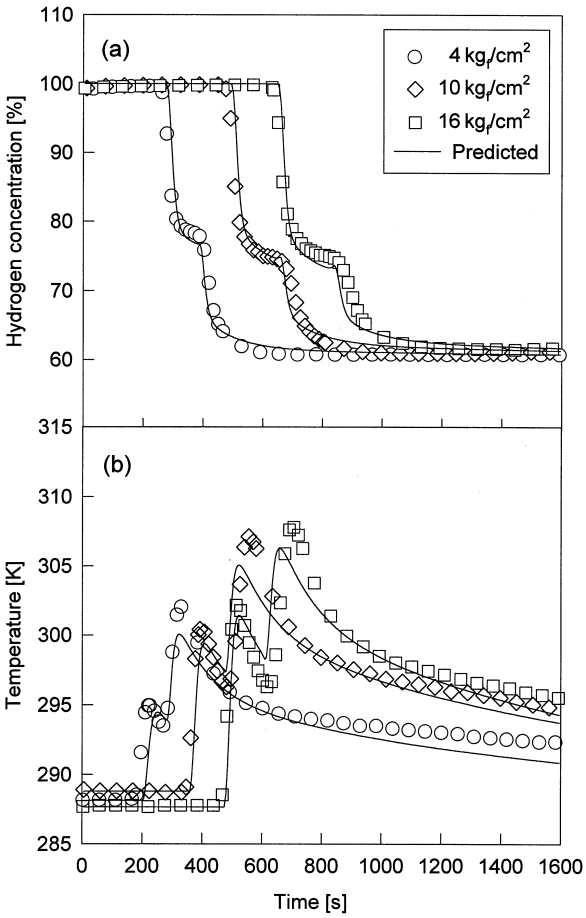

Figure 11. (a) Effect of adsorption pressure on H_2 breakthrough curves at constant 6.8 LSTP/min feed flow rate and (b) corresponding temperature profiles in the activated carbon bed.

MARCEL DEKKER, INC.
270 Madison Avenue, New York, New York 10016

As shown in Fig. 10(a), the inflection and tailing of H_2 breakthrough curve became prominent as the feed flow rate was decreased. As the feed flow rate became lower, the contact time of each component became longer. Since the interaction between the adsorbate and the adsorbent in the bed increased in proportion to the contact time, the concentration wave fronts of CO and CH_4 became further apart. Therefore, the plateau of CO became wide as shown in Fig. 4. Figure 10(b) shows the corresponding temperature excursion at the position of 75 cm from the feed end. Since, at 9 LSTP/min, concentration wave fronts of CO and CH_4 became close with an increase in feed flow rate, the heat generation by the adsorption of CO and CH_4 took place at short intervals. Therefore, the maximum increase in temperature at higher flow rate was greater than that at lower flow rate.

In Fig. 11, since the difference in the adsorption capacity of CO and CH_4 on the activated carbon increased with an increase in the adsorption pressure, two concentration wave fronts were separated further apart and the roll-up of CO by CH_4 was increased. Therefore, the ravine between the two temperature peaks got deeper due to more heat transfer through the wall in Fig. 11(b). As shown in Fig. 11(a), the inflection point of H_2 breakthrough curve was lowered, and the extent of inflection became slightly steeper with an increase in the adsorption pressure due to further separation of both concentration wave fronts and an increase in the CO roll-up.

Another interesting feature in Figs. 10 and 11 is the breakthrough time. In Fig. 10, breakthrough time was not decreased linearly as feed flow rate was increased linearly. This implies that at least a certain amount of contact time is required due to the mass transfer resistance in the adsorbent. Therefore, the increase in contact time made the system adsorb the feed gas sufficiently and led to low velocity in MTZ. Also, the breakthrough time was not elongated linearly with a linear increase in the adsorption pressure in Fig. 11. This implies that adsorption equilibrium approaches a limiting equilibrium amount. Since MTZ velocity was a function of interstitial velocity, bed voidage and equilibrium adsorption gradient, MTZ velocity and breakthrough time were not changed linearly despite a linear change in flow rate or adsorption pressure.

Figures 12 and 13 show the effects of feed flow rate and adsorption pressure on breakthrough curves in a zeolite bed, respectively. Since the breakthroughs of both CH_4 and CO occurred almost simultaneously as mentioned in Fig. 6, there was no inflection in the H_2 breakthrough curves and only one peak in the temperature excursion. Also the H_2 breakthrough curves dropped very steeply due to a sharp CH_4 wave front as shown in Fig. 9. Similar to the activated carbon bed, breakthrough time did not vary linearly despite a linear change in feed flow rate and adsorption pressure. Also, the elongation by the feed flow rate and adsorption pressure in the zeolite 5A bed was smaller than that in the activated carbon bed.

MARCEL DEKKER, INC.
270 Madison Avenue, New York, New York 10016

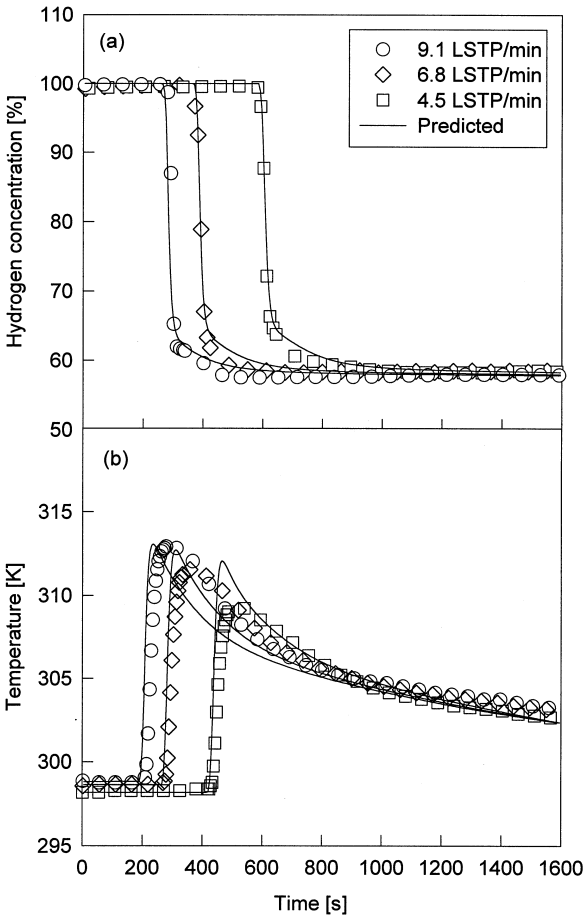

Figure 12. (a) Effect of feed flow rate on H_2 breakthrough curves at constant 10 kg_f/cm^2 adsorption pressure and (b) corresponding temperature profiles in the zeolite 5A bed.

MARCEL DEKKER, INC.
270 Madison Avenue, New York, New York 10016

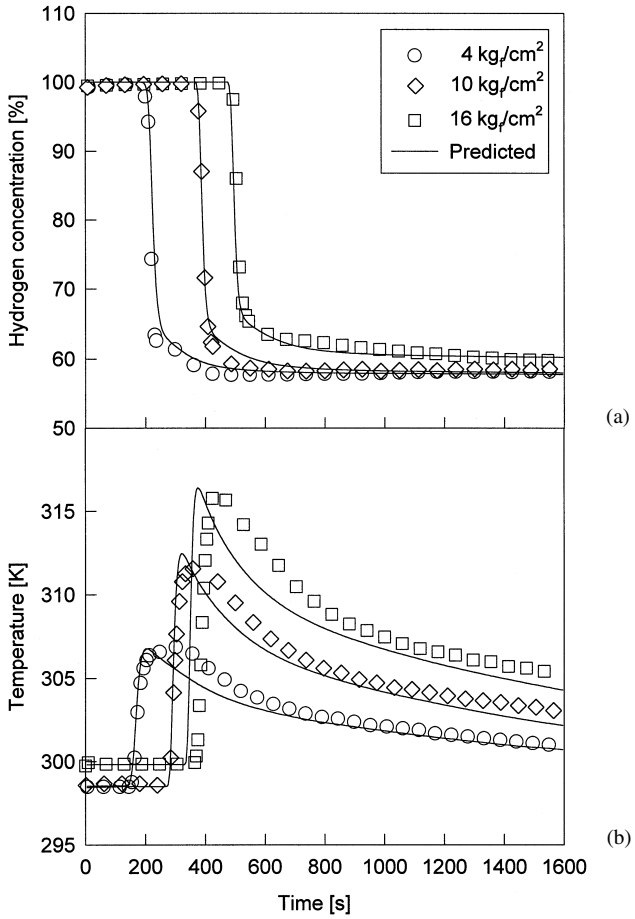

Figure 13. (a) Effect of adsorption pressure on H_2 breakthrough curves at constant 6.8 LSTP/min feed flow rate and (b) corresponding temperature profiles in the zeolite 5A bed.

CONCLUSIONS

The adsorption dynamics and thermal effects on breakthrough curves in the activated carbon bed and zeolite 5A bed were compared by using hydrogen ternary mixture (H_2/CH_4/CO; 60.4:28.1:11.5 vol%) as feed gas in the range of 4–16 kg$_f$/cm^2 adsorption pressure and 4.5–9.1 LSTP/min feed flow rate. The roll-up of CO and separation of mass transfer zones between CO and CH_4 led to a stepwise breakthrough curve of H_2 in the activated carbon bed. The plateau of the CO roll-up in the non-isothermal and non-adiabatic conditions showed some slope

MARCEL DEKKER, INC.
270 Madison Avenue, New York, New York 10016

that was different from those in the isothermal and adiabatic conditions. Since these results came from two temperature excursions with a deep ravine, the temperature in the bed affected each concentration profile of CO and CH_4. As a result, the inflection of H_2 breakthrough curve became prominent as the flow rate decreased. Since the wide separation of CO and CH_4 wave fronts made the ravine of two temperature peaks go deeper, the tailing of H_2 increased with a decrease in feed flow rate. Also, the inflection point of H_2 breakthrough curve was lowered, and the extent of inflection became slightly steeper with an increase in the adsorption pressure. However, since both wave fronts of CH_4 and CO in the zeolite bed proceeded almost simultaneously, there was a small roll-up of CH_4 and a wide breakthrough of CO. Also, the small inflection of H_2 breakthrough curve occurred at the roll-up of CH_4 without the separation of temperature excursion. The extent of CH_4 roll-up in the non-isothermal and non-adiabatic condition was smaller than that in both isothermal and adiabatic conditions because of heat transfer effects. Also, the effect of feed flow rate and adsorption pressure on the breakthrough behavior in the zeolite 5A bed was less significant than that in the activated carbon bed.

In summary, the roll-up behavior depended on the affinity difference between CO and CH_4 in an adsorbent as well as on the bed temperature profile. Each of concentration wave fronts could be controlled by using a combined bed with various adsorbents because each concentration wave front propagated with its own wave front velocity in each adsorbent by different adsorption equilibrium and heat of adsorption.

NOMENCLATURE

A	cross-sectional area (m^2)
B	Langmuir-Freudlich isotherm parameter (1/atm)
C_p	heat capacity (J/kg/K)
D	diffusivity (cm^2/s)
D_L	axial dispersion coefficient (m^2/s)
h	heat transfer coefficient ($J/m^2/s/K$)
K_L	effective axial thermal conductivity (J/m/s/K)
L	bed length (cm)
n	Langmuir-Freudlich isotherm parameter
P	pressure (kg_f/cm^2)
$\bar{q}$	volume-averaged adsorbed phase concentration (mol/kg)
q^*	equilibrium adsorbed-phase concentration (mol/kg)
q_m	Langmuir-Freundlich isotherm parameter (mol/g)
Q	average isosteric heat of adsorption (J/mol)
R	radius (m)

MARCEL DEKKER, INC.
270 Madison Avenue, New York, New York 10016

Re	Reynolds number, $\rho_g \nu(2R_p)/\mu$
Sc	Schmidt number, μ / ρ_g / D
t	time (s)
T	solid-phase and gas-phase temperature (K)
T_{atm}	ambient temperature (K)
u	interstitial velocity (m/s)
v	superficial velocity (m/s)
z	axial position in an adsorption bed (m)

Greek Symbols

ε	bed voidage
ε_t	total void fraction
ρ	density (cm^3/g)
μ	viscosity (cm/g/s)
ν	superficial velocity (cm/s)
ω	LDF coefficient (1/s)

Subscripts

B	bed
i	component i, inner
p	pellet
g	gas phase
o	outer
s	solid phase
w	wall

ACKNOWLEDGMENT

The financial assistance and support of BK21 is gratefully acknowledged.

REFERENCES

1. Kumar, R. Adsorption Process for Recovering Two High Purity Gas Products from Multicomponent Gas Mixtures. US Patent 4,913,709, April 3, 1990.

2. Chlendi, M.; Tondeur, D. Dynamic Behaviour of Layered Columns in Pressure Swing Adsorption. Gas. Sep. Purif. **1995**, *9* (4), 231–242.
3. Pigorini, G.; LeVan, M.D. Equilibrium Theory for Pressure Swing Adsorption. 2. Purification and Enrichment in Layered Beds. Ind. Eng. Chem. Res. **1997**, *36*, 2296–2305.
4. Malek, A.; Farooq, S. Hydrogen Purification from Refinery Fuel Gas by Pressure Swing Adsorption. AIChE J. **1998**, *44* (9), 1985–1992.
5. Lee, C.-H.; Yang, J.; Ahn, H. Effects of Carbon-to-Zeolite Ratio on Layered Bed H2 PSA for Coke Oven Gas. AIChE J. **1999**, *45* (3), 535–545.
6. Ahn, H.; Lee, C.-H.; Seo, B.; Yang, J.; Baek, K. Backfill Cycle of a Layered Bed H2 PSA Process. Adsorption **1999**, *5*, 419–433.
7. Sircar, S.; Kumar, R. Adiabatic Adsorption of Bulk Binary Gas Mixtures. Ind. Eng. Chem. Process Des. Dev. **1983**, *22*, 271–280.
8. Sircar, S.; Kumar, R. Column Dynamics for Adsorption of Bulk Binary Gas Mixtures on Activated Carbon. Sep. Sci. Technol. **1986**, *21*, 919–939.
9. Hwang, K.S.; Jun, J.H.; Lee, W.K. Fixed-bed Adsorption for Bulk Component System. Non-equilibrium, Non-isothermal and Non-adiabatic Model. Chem. Eng. Sci. **1995**, *50* (5), 813–825.
10. Silva, J.A.C.; Rodrigues, A.E. Fixed-Bed Adsorption of Two Linearly Adsorbed Components in Presence of an Inert. Chem. Eng. Sci. **1998**, *53* (20), 3513–3520.
11. Park, J.-H.; Kim, J.-N.; Cho, S.-H.; Kim, J.-N.; Yang, R.T. Adsorber Dynamics and Optimal Design of Layered Beds for Multicomponent Gas Adsorption. Chem. Eng. Sci. **1998**, *53* (23), 3951–3963.
12. Yang, J.; Lee, C.-H. Adsorption Dynamics of a Layered Bed PSA for H2 Recovery from Coke Oven Gas. AIChE J. **1998**, *44* (6), 1325–1334.
13. Farooq, S.; Ruthven, D.M. Dynamics of Kinetically Controlled Binary Adsorption in a Fixed Bed. AIChE J. **1991**, *37* (2), 299–301.
14. Doong, S.J.; Yang, R.T. Bulk Separation of Multicomponent Gas Mixtures by Pressure Swing Adsorption: Pore/Surface Diffusion and Equilibrium Models. AIChE J. **1986**, *32* (3), 397–410.
15. Wakao, N.; Funazkri, T. Effect of Fluid Dispersion Coefficients on Particle-to-Fluid Mass Transfer Coefficients in Packed Beds. Chem. Eng. Sci. **1978**, *33*, 1375–1384.
16. Malek, A.; Farooq, S. Study of a Six-Bed Pressure Swing Adsorption Process. AIChE J. **1997**, *43* (10), 2509–2523.
17. Kim, W.-G.; Yang, J.; Han, S.; Cho, C.; Lee, C.-H.; Lee, H. Experimental and Theoretical Study on H2/CO2 Separation by a Five-Step One-Column PSA Process. Korean J. Chem. Eng. **1995**, *12*, 503–511.
18. Wu, J.C.; Fan, L.T.; Erickson, L.E. Three-Point Backward Finite Difference Method for Solving a System of Mixed Hyperbolic-Parabolic Partial Differential Equations. Comput. Chem. Eng. **1990**, *14*, 679–685.

MARCEL DEKKER, INC.
270 Madison Avenue, New York, New York 10016

19. Jee, J.; Chun, C.; Kim, M; Lee, C.-H. Adsorption Characteristics of Hydrogen Mixture in Layered Bed: Binary, Ternary and 5-Component Mixtures. Ind. Eng. Chem. Res. **2001**, *40*, 868–878.

Received May 2000
Revised October 2000

Request Permission or Order Reprints Instantly!